

Chapter 1

Monte Carlo Event Generators

General-purpose Monte Carlo (GPMC) generators like PYTHIA 6 and PYTHIA 8 [1,2], HERWIG [3], HERWIG++ [4], and SHERPA [5], provide fully exclusive modeling of high-energy collisions. They play an essential role in data analysis, where they are used together with detector simulation to provide a realistic estimate of the detector response to collision events, and in the planning of new experiments, where they are used to estimate signals and backgrounds in high energy processes. They are built by several components, that can be thought of as describing the physics starting from the very short distance scales, up to the typical scale of hadron formation and decay. Since QCD is weakly interacting at short distances (i.e., distances much below a femtometer), and strongly interacting at large distances, the components of the GPMC dealing with the shortest distances are based upon perturbation theory. At larger distances, all soft hadronic phenomena, like hadronization and the formation of the underlying event, cannot be computed in a sound theoretical way, and one must rely upon QCD inspired models.

The purpose of this review is to illustrate the main components of these generators. It is divided into two four sections. The first section deals with short-distance, perturbative phenomena. The basic concepts leading to the simulations of the dominant QCD processes are illustrated here.

In the second section, hadronization phenomena are treated. The two most popular hadronization models for the formation of primary hadrons, the string and cluster models, are illustrated. The basics of the implementation of primary-hadron decays into stable ones is also illustrated here.

In the third section, models for soft hadron physics are discussed. These include models for the underlying event, and for minimum-bias interactions. Issues on Bose-Einstein and color-reconnection effects are also discussed here.

The fourth section deals with tuning. In essence, the “model” part of the GPMC contains several parameters that must be fixed by tuning the model to real data. The basics of the tuning procedure is given here.

1.1 Short-distance physics in GPMC generators

The short-distance component of a GPMC generator deals with the computation of the primary process at hand, and with the generation of the radiation of colored partons (and eventually also of photons) on time scales that are well below $1/\Lambda$, where with Λ denotes a typical hadronic scale of few hundred MeV.¹ In e^+e^- annihilation, for example, the short-distance physics describes the evolution of the system from the instant when the e^+e^- pair annihilates up to a time when the size of the produced system is well below a femtometer. Below this scale, thanks to asymptotic freedom, one can apply QCD perturbation theory.

The primary process itself must be a short-distance process. This is obviously the case for electroweak or strong production of massive particles, where the scale is the Compton wavelength of the produced objects, for the production of light parton pairs in e^+e^- annihilation and for the production of light partons with large transverse momenta in hadronic collisions, the scale in the last two cases being the wavelength of the outgoing partons. In the present discussion we will call Q the momentum scale of the primary process, with $Q \gg \Lambda$, so that the corresponding time and distance scale $1/Q$ is small. QCD corrections to the primary process are in general not small, that is to say, they are not of order $\alpha_s(Q)$. This is due to the presence of collinear and infrared singularities in QCD. Thus, for example, a QCD correction in which a parton from the primary interaction splits into two partons of comparable energy, is of order $\alpha_s(Q) \log(Q/\Lambda)$ (where Λ is a typical hadronic scale). This is because the parton splitting process is logarithmically divergent at small angles, with the logarithm being cut off by some effective hadron mass. Since $\alpha_s(Q)$ is of the order of $1/\log(Q/\Lambda)$, the corresponding cross section receives a correction of order unity. These large corrections build up to all orders in perturbation theory. Thus for example, two subsequent collinear splittings yield $\alpha_s^2(Q) \log^2(Q/\Lambda)$. Therefore, corrections of order 1 arise to all orders in perturbation theory. The dominant region of phase space is the one where radiation is strongly ordered by angles. This means that, from a typical final-state configuration, by clustering together final-state parton pairs with the smallest angle recursively, we can reconstruct a unique branching tree, that may be view as the splitting history of the event. Thus, in the dominant region, there is a one-to-one correspondence between final-state configurations and splitting histories. The ordering in angles can also be viewed as ordering in virtualities, or transverse momenta. In fact, in the small angle limit, the virtuality of a parton of energy E , splitting into two on-shell partons is given by

$$t = E^2 z(1-z)(1-\cos\theta) \approx E^2 z(1-z) \frac{\theta^2}{2} \quad (1.1)$$

where E is the energy of the incoming parton, and z and $1-z$ are the energy fractions carried by the produced partons; the transverse momentum of the final partons relative to the direction of the incoming one is instead given by

$$p_T^2 \approx E^2 z^2(1-z)^2 \theta^2. \quad (1.2)$$

So, strong ordering in angle, in virtuality or in transverse momenta are equivalent in the dominant region, unless we need to consider the regions with very small z or $1-z$ values.

¹In this discussion we use natural units such that $c = 1$ and $\hbar = 1$, with energy, momenta and masses measured in eV, and time and distances measured in eV^{-1} .

In QCD, because of soft divergences, these regions are in fact important, and the choice of the appropriate ordering variable is very relevant. We postpone the discussion of the soft problem to the following sections.

The so called KLN theorem [6, 7] guarantees that large logarithmically divergent corrections, arising from final-state collinear splitting and from soft emissions, cancel against the virtual corrections in the total cross section, order by order in perturbation theory. Furthermore, the factorization theorem guarantees that initial-state collinear singularities can be factorized into the parton density functions. Therefore, at the end, the cross section for the basic process remains accurate up to corrections of higher orders in $\alpha_S(Q)$, provided it is interpreted as an inclusive cross section, rather than in terms of a bare partonic cross section. Thus, for example, the leading order cross section for $e^+e^- \rightarrow q\bar{q}$ is a good leading order estimate of the e^+e^- cross section for the production of a pair of quarks accompanied by an arbitrary number of collinear and soft gluons, but is not a good estimate of the cross section for the production of a $q\bar{q}$ pair with no extra radiation.

Shower Monte Carlo algorithms are used to compute the cross section for generic hard processes including all leading logarithmic corrections. These algorithms initiate the shower process with the generation of the kinematics of the basic process, performed with a probability proportional to its leading order partonic cross section. This leading order partonic cross section is to be interpreted physically as the inclusive cross section for the basic process, followed by an arbitrary sequence of small angle splitting processes. A probability is then assigned to each splitting sequence. Thus, the initial leading order cross section is parted into the cross sections for a multitude of final states of arbitrary multiplicity. The sum of all these cross sections yields again the cross section of the primary process. This property of the GPMCs reflects the KLN cancellation mentioned earlier, and it is often called “unitarity of the shower process”, a name that reminds us that the KLN cancellation is itself a consequence of unitarity. The fact that a quantum mechanical process can be described in terms of composition of probabilities, rather than amplitudes, follows from the leading logarithmic approximation. In fact, in the dominant, strongly ordered region, subsequent splittings are separated by increasingly large times and distances, and this suppresses interference effects.

We now illustrate the basic parton shower algorithm, as first introduced in ref. [8]. The purpose of this illustration is to give a schematic representation of how shower algorithms works, to introduce some concept that will be referred to in the following, and to show the relationship between shower algorithms and Feynman diagrams computations. We consider for simplicity the example of e^+e^- annihilation into $q\bar{q}$ pairs. With each dominant (i.e. strongly ordered) final-state configuration one can associate a unique ordered tree diagram, by clustering together recursively final-state parton pairs with the smallest angle, and ending up with the hard production vertex (i.e. the $\gamma^* \rightarrow q\bar{q}$). The momenta of all intermediate lines of the tree diagram are then uniquely determined from the final-state momenta. Virtualities in the graph are also strongly ordered. One assigns to each splitting vertex a virtuality t , that equals the invariant mass of the pair of generated partons, the energy fractions z and $1-z$ of the two generated partons, and an azimuth ϕ of the splitting process with respect the the momentum of the incoming parton. We assume for definiteness that z and ϕ are defined in the centre-of-mass frame of the e^+e^- collision, although several different definitions are possible that differ only beyond the leading logarithmic approximation. The differential cross section for a given final state is given by the product of the differential cross section for the

initial $e^+e^- \rightarrow q\bar{q}$ process, multiplied by a factor

$$\Delta_i(t, t') \frac{\alpha_s(t)}{2\pi} P_{i,jk}(z) \frac{dt}{t} dz \frac{d\phi}{2\pi}. \quad (1.3)$$

for each intermediate line ending in a splitting vertex. We have denoted with t' the maximal virtuality that is allowed for the line, t is the virtuality assigned to its final extreme, and z and ϕ refer to the splitting process at the final extreme. $\Delta(t, t')$ is the so called Sudakov form factor

$$\Delta_i(t, t') = \exp \left[- \int_t^{t'} \frac{dq^2}{q^2} \frac{\alpha_s(q^2)}{2\pi} \sum_{jk} P_{i,jk}(z) dz \frac{d\phi}{2\pi} \right], \quad (1.4)$$

The suffix i represent the parton specie of the incoming parton, and jk those of the final parton, and $P_{i,jk}(z)$ are the Altarelli-Parisi [9] splitting kernels. Final-state lines that do not undergo any further splitting are given the factor $\Delta_i(t_0, t')$ and nothing else, where t_0 is an infrared cutoff for collinear splitting.

Notice that the definition of the Sudakov form factor is such that

$$\Delta_i(t_2, t_1) + \int_{t_2}^{t_1} \frac{dt}{t} dz \frac{d\phi}{2\pi} \sum_{jk} \Delta_i(t, t_1) \frac{\alpha_s(t)}{2\pi} P_{i,jk}(z) = 1. \quad (1.5)$$

This implies that the cross section for developing the shower up to a given stage does not depend upon what will happen next, since subsequent factors for further splitting or not splitting add up to one. One can then formulate the shower cross section in a probabilistic way along the following lines. The Sudakov form factor $\Delta_i(t_2, t_1)$ is interpreted as the probability for a splitting not to occur, for a parton of type i , starting from a branching vertex at the scale t_1 , down to a scale t_2 . Notice that $0 < \Delta_i(t_2, t_1) \leq 1$, where the upper extreme is reached for $t_2 = t_1$, and the lower extreme for $t_2 = t_0$. From eq. 1.4, it seems that the Sudakov form factor would become 0 if $t_2 = 0$. On the other hand, because of the presence of the running coupling constant in the integrand, t_2 cannot be taken smaller than some cutoff scale of the order of Λ_{QCD} , so that at its lower extreme the Sudakov form factor is small, but not zero. Event generation then proceeds as follows. One gets a uniform random number $0 \leq r \leq 1$, and seeks a solution of the equation $r = \Delta_i(t_2, t_1)$ as a function of t_2 . If r is too small and no solution exists, no splitting is generated, and the line is interpreted as a final parton. If a solution t_2 exists, a branching is generated at the scale t_2 . Its z value and the final parton species jk are generated with a probability proportional to $P_{i,jk}(z)$. The azimuth is instead generated uniformly. This procedure is started with both the initial quark and the antiquark, thus producing two shower cascades. It may generate an arbitrary number of partons, and it stops when no final-state partons undergo further splitting.

It can be shown that the shower cross section described above is obtained from perturbative QCD by keeping only the collinear-dominant real and virtual contributions to the cross section. In particular, up to terms that vanish after azimuthal average, the product of the cross section for the basic process, times the factors

$$\frac{\alpha_s}{2\pi} \frac{dt}{t} dz \frac{d\phi}{2\pi} \quad (1.6)$$

at each branching vertex, gives the leading logarithmic contribution to the real cross section for the same process (where the logarithms arise from the dt/t integrations). Dominant virtual corrections in the same approximation are provided by the running coupling at each vertex and by the Sudakov form factors.

1.1.1 Angular correlations

In gluon splitting processes ($g \rightarrow q\bar{q}$, $g \rightarrow gg$) in the collinear approximation, the distribution of the splitted pair is not uniform in angle, and the Altarelli-Parisi splitting functions is recovered only after azimuthal average. This azimuthal dependence is due to the interference of positive and negative helicity states for the gluon that undergoes splitting. Spin correlations propagate through the shower generation, and determine acausal correlations of the EPR kind [10]. A method to partially account for azimuthal correlations was introduced in ref. [11]. With this method the azimuthal correlation between two successive splitting is computed by averaging over polarization, and is then applied at each branching step. Acausal correlations are argued to be small, and are discarded with this method, that is still presently used in the PYTHIA code [1]. A method that fully includes spin correlation effects was later proposed by Collins [12], and has been implemented in the fortran HERWIG code [13].

1.1.2 Initial-state radiation

Initial-state radiation arises because incoming partons can radiate off collinear partons before entering the hard scattering process. In doing so, their virtuality becomes negative, and the dominant logarithmic region is the one where virtualities become larger and larger in absolute value with each collinear emission, until the parton enters the hard scattering process. Its virtuality is limited by the hardness of the basic process itself. A shower algorithm that goes from large to small virtualities would thus work backward in time for initial state radiation. An appropriate algorithm was introduced in ref. [14], and was basically adopted in all shower models.

1.1.3 The soft-emission problem

In field theories like QCD, there are two sources of large logarithms of infrared origin. One has to do with collinear singularities, that arise when two final-state particles become collinear, or when a final-state particle becomes collinear to an initial-state one. The other has to do with the emission of soft gluons at arbitrary angles. Because of that, it turns out that in QCD perturbation theory two powers of large logarithms can arise for each power of α_s . The expansion in leading soft and collinear logarithms is often referred to as the double logarithmic expansion.

The traditional parton-shower algorithm of ref. [8] is focussed upon collinear singularities. The logarithms arising from soft gluon emission show up as divergences in the z integration of the Altarelli parisi splitting kernels $P_{i,jk}(z)$. In other words, the formalism only captures the soft logarithms that are associated with collinear ones, i.e. only the soft logarithms of the double log region. However, even getting correctly the double logarithmic structure is

not a totally trivial task. It was shown in a sequel of publications [15–18] that in order to represent correctly the double logarithmic region one should choose as the ordering variable t the splitting angle, rather than the virtuality of the splitting pair, and that the argument of α_s at the splitting vertex should be taken equal to the relative parton transverse momentum after the splitting. With this choice, destructive coherent interference arising from large angle soft emission from a bunch of collinear partons is automatically taken into account. Without properly accounting for this destructive interference, the parton multiplicity has a larger growth with energy, which in turn leads to a larger growth of hadron multiplicity in the complete shower model, a growth that is clearly inconsistent with the observed multiplicity growth in e^+e^- colliders. For this reason, some kind of angular ordering was adopted in most parton-shower models.

1.1.4 Dipole shower models

A radical alternative for dealing with the soft problem has been put forward in refs. [19–21]. If one focusses upon soft emission, rather than collinear emission, it becomes natural to consider a branching process where it is a parton pair (i.e. a dipole) rather than a single parton, that emits a soft parton. This approach allows one to get the correct logarithmic structure for soft emission in the large- N_c limit. Within this method it is also possible to recover the correct collinear singularity structure when the emitted parton is no longer soft, and is collinear to either partons in the dipole.

A number of variants of this method have appeared in the literature, mostly in an attempt to devise shower algorithm that can be easily matched to NLO calculations. They thus use a shower approximation that has the same form of counterterms that are used in standard subtraction method for NLO calculations. We quote in particular the showers based upon the antenna subtraction method [22–24], and those based upon dipole subtraction [25, 26]. The latter in particular is implemented in the SHERPA Shower Monte Carlo [27].

The PYTHIA and SHERPA GPMC programs implement a dipole type shower.

1.1.5 Massive quarks

Quark masses act as cut-off on collinear singularities. If the mass of a quark is below, or of the order of Λ_{QCD} , its effect in the shower is small, since the shower is stopped when it reaches scales of that order. If the mass is larger than Λ_{QCD} , like in c or b production, it is the mass, rather than the typical hadronic scale, that cuts off collinear radiation. On this ground, we thus expect less collinear activity for heavy quarks rather than light ones. In other words, heavy quarks radiate less, and this is the reason why they carry a large fraction of the momentum acquired in the hard production process. Therefore, a shower algorithm must limit the emission angle from a massive quark. For a quark of energy E and mass m , when $\theta \leq m/E$ the divergent behaviour $d\theta/\theta$ of the collinear splitting function must stop. This feature can be implemented with different levels of sophistication. Using the fact that soft emission exhibits a zero at zero emission angle, older parton shower algorithms simply limited the shower emission to be not smaller than the angle θ_0 . More modern approaches are described in ref. [28], where mass effects are included using a kind of matrix element correction method, and in ref. [29], where a generalization of the Altarelli-Parisi splitting

kernel is found in the case of massive quarks. This last method is used in HERWIG++ and SHERPA, while the former is used in PYTHIA 8.

1.1.6 The high energy limit

Shower MC models are based upon the resummation of enhanced contributions that arise from the collinear regions and from the soft regions of phase space. A new kind of dominant contribution arises when we consider a production process involving scales much above the strong interaction scale, but yet much below the total available energy. The large rapidity gaps that become available in the production phase space in this limit yield also a different kind of enhanced contribution. This regime is often referred to as the semi-hard regime, or as the high energy limit, or as the small x regime, since the typical value of momentum fractions involved in the parton densities are small. Considering, for example, the production of a not-so-heavy system, like a $b\bar{b}$ pair, or a pair of jets with small invariant mass, we know that its rapidity distributions covers a large rapidity plateau. If we now consider the emission of an extra gluon with a transverse momentum comparable to the b mass, while this process will cost an extra power of α_S , a phase space factor of the order of the rapidity plateau available to the gluon will enhance the cross section. Since the width of the rapidity plateau is of order $\log(E/m)$ (where m is the mass of the not-so-heavy system and E is the hadronic CM energy), contributions of order $(\alpha_S \log(E/m))^n$ may become important for all values of n , thus requiring a resummation procedure. Unlike the collinear or soft regime, here we have an enhancement associated to large rapidity separation (and thus large invariant mass) for pairs of partons. Resummation of these effects leads to cross section that grow like a small (i.e. of the order of the strong coupling constant) power of the ratio E/m . The BFKL formalism [30–33] describes this power growth, associating it with the Regge behaviour due to the exchange of a perturbative Pomeron. Standard GPMC programs do not generally include these enhanced contributions. There are, however, specialized generators that address this problem, according to different approaches. The CASCADE Monte Carlo [34, 35] is based upon the CCFM equation, a modification of the evolution of the parton shower that accounts for small x effects [36–38]. CASCADE uses backward evolution for initial-state radiation, at variance with SMALLX, a previous implementation of the CCFM approach that used forward evolution [39, 40]. The ARIADNE implementation of ref. [41], referred to as the LDCMC, was based instead on the linked dipole chain model, introduced in [42, 43]. In refs. [44–46] an algorithm was developed for computing scattering amplitudes in the kinematic regime where final-state partons have large rapidity separation. These amplitudes are convoluted with standard parton density functions in order to compute physical cross sections. In ref. [47] a method has been proposed to interface these cross section to the ARIADNE shower model without overcounting.

When the scale of the hard process approaches the typical QCD scales, semihard physics should merge smoothly with soft physics. This suggests the possibility to describe minimum bias collisions within a semi-hard framework. Besides using the BFKL equation to resum leading semihard logarithms, one should also consider in this case the onset of saturation effects, that limit the power growth of the cross sections. It happens in fact that the power growth in E/m violates unitarity bounds at some point. Saturation mechanisms become then active, and restore unitarity. The very recent DIPSY [48] Monte Carlo aims at a

description of non-diffractive, minimum bias physics, based upon the QCD description of semihard processes. It uses the dipole description of semihard physics due to Mueller [49–51], that, besides reproducing the BFKL growth of the cross sections, allows for a simpler understanding of saturation and unitarity restoration.

1.1.7 Electromagnetic corrections

The physics of photon emission from light charged particles can also be treated with a shower MC algorithm. A high energy electron, for example, is always accompanied by brehmstrahlung photons, that affect considerably its dynamics. Also here, similarly to the QCD case, electromagnetic corrections, are of order $\log Q/m_e\alpha_{\text{em}}$, so that their inclusion in the simulation process is mandatory. This can be done with a Monte Carlo algorithm. In case of photons emitted by leptons, at variance with the QCD case, the shower can be continued down to values of the lepton virtuality that are arbitrarily close to its mass shell. For photons emitted from quarks, we have instead the obvious limitation that the photon wavelength cannot exceed the typical hadronic size. Longer wavelength photons are in fact emitted by final-state hadrons, rather than quarks. This last effect is in practice never modelled by existing shower MC implementations.

In practice, photon radiation must be cut-off below a certain energy, in order for the shower algorithm to terminate. Therefore, there is always a minimum energy for emitted photons that depends upon the implementations. In case of electrons, this scale is typically of the order of the mass of the electron. Electromagnetic radiation below this scale is no longer enhanced by collinear singularities, and is thus bound to be soft, so that the electron momentum is not affected by it. On the other hand, electromagnetic radiation from quarks is cut off at a typical hadronic scale. At this scale, in fact, radiation from quarks would add up coherently to form the radiation from final-state hadrons.

1.1.8 Beyond the Standard Model Physics

The inclusion of processes for physics beyond the Standard Model in event generators is to some extent just a matter of implementing the relevant hard processes and (chains of) decays, with the level of difficulty depending on the complexity of the model and the degree of automation [52, 53]. Notable exceptions are long-lived colored particles [54], particles in exotic color representations [55–57], and particles showering under new gauge symmetries [58]. Further complications that may be relevant are finite-width effects (discussed in section 1.1.9) and the assumed threshold behavior.

In addition to code-specific implementations [59], there are a few commonly adopted standards that are useful for transferring information and events between codes. Currently, the most important of these is the Les Houches Event File (LHEF) standard [60], normally used to transfer parton-level events from a hard-process generator to a shower generator. Another important standard is the Supersymmetry Les Houches Accord (SLHA) format [61], originally used to transfer information on supersymmetric particle spectra and couplings, but by now extended to apply also to more general BSM frameworks and incorporated within the LHEF standard [62].

1.1.9 Decay Chains and Particle Widths

In most BSM processes and some SM ones, an important aspect of the event simulation is how decays of short-lived particles, such as top quarks, EW and Higgs bosons, and new BSM resonances, are handled. We here briefly summarize the spectrum of possibilities, but emphasize that there is no universal standard. Users are advised to check whether the treatment of a given code is adequate for the physics study at hand.

The appearance of an unstable resonance as a physical particle at some intermediate stage of the event generation implies that its production and decay processes are treated as being factorized. This is valid up to corrections of order Γ/m_0 , with Γ the width and m_0 the pole mass. States whose widths are a substantial fraction of their mass should not be treated as “physical particles”, but rather as intrinsically off-shell internal propagator lines.

For states treated as physical particles, two aspects are relevant: the mass distribution of the decaying particle itself and the distributions of its decay products. For the former, matrix-element generators often use a simple δ function at m_0 . The next level up, typically used in GPMCs, is to use a Breit-Wigner distribution (relativistic or non-relativistic), which formally resums higher-order virtual corrections to the mass distribution. Note, however, that this still only generates an improved picture for *moderate* fluctuations away from m_0 . Similarly to above, particles that are significantly off-shell (in units of Γ) should not be treated as resonant, but rather as internal off-shell propagator lines. In most GPMCs, further refinements are included, for instance by letting Γ be a function of m (“running widths”) and by limiting the magnitude of the allowed fluctuations away from m_0 .

For the distributions of the decay products, the simplest treatment is again to assign them their respective m_0 values, with a uniform phase-space distribution. A more sophisticated treatment distributes the decay products according to the differential decay matrix elements, capturing at least the internal dynamics and helicity structure of the decay process. Further refinements include polarizations of the external states [63] and assigning the decay products their own Breit-Wigner distributions, the latter of which opens the possibility to include also intrinsically off-shell decay channels.

When computing partial widths and/or modifying decay tables, one should be aware of the danger of double-counting channels involving intermediate on-shell particles, see section 1.2.3.

1.1.10 Matching with Matrix Elements

The shower algorithm is based upon a combination of the collinear (small angle) and soft (small energy) approximation. It is thus inaccurate for hard, large angle emissions. It also lacks NLO corrections to the basic process, since those require that the hardest emission is treated with at least leading order accuracy, and that exact NLO virtual corrections are included.

Traditional GPMCs, like HERWIG and PYTHIA, have included since a long time the so called Matrix Element Corrections (MEC) [20, 64–67] to the simplest basic processes, like vector boson and Higgs production (i.e. $2 \rightarrow 1$ processes) and top decays ($1 \rightarrow 2$ processes). The MEC corrects the emission of the hardest jets at large angles, so that it becomes exact at leading order.

In the past decade, considerable progress has taken place in order to improve the parton shower description of hard collisions, in two different directions: the so called Matrix Elements and Parton Shower matching (ME+PS from now on), and the matching of NLO calculations and Parton Showers (NLO+PS).

The ME+PS methods allows one to use exact tree-level matrix elements for hard, large angle emissions. It was first formulated in the so called CKKW paper [68], in the context of e^+e^- annihilation into hadrons. It has been extended to hadronic collisions in [69]. In [70] a matching procedure appropriate to dipole shower models has been considered. Several variants of the CKKW approach have also been proposed the so called CKKW-L method [71], the pseudoshowers method [72] and the MLM matching procedure (see [73] for a description of it). In [74] the need of truncated showers has been pointed out. These are needed in order to maintain colour coherence when interfacing matrix element calculations to angular ordered parton showers.

In the ME+PS method one typically starts by generating exact matrix element for the production of the basic process plus a certain number $\leq n$ of other partons. A minimum separation is required for the produced partons, requiring, for example, that the relative transverse momentum in any pair of partons is above a given cut Q_0 . One then reweights these amplitudes in such a way that, in the strongly ordered region, the virtual effects that are included in the shower algorithm (i.e. running coupling and Sudakov form factors) are also accounted for. At this stage the generated configurations are tree-level accurate at large angle, and at small angle they match the shower algorithms results, except that there are no emissions below the scale Q_0 , and no final states with more than n partons. These kinematic configurations are thus fed into a GPMC. The GPMC must generate all splitting with relative transverse momentum below the scale Q_0 , for initial events with less than n partons, or below the scale of the smallest pair transverse momentum, for events with exactly n partons. The matching parameter Q_0 must be chosen to be large enough for perturbation theory to hold, but smaller than the clustering jet parameter that is used in analyzing the events. Notice that MEC are equivalent to ME+PS generators with $n = 1$, with the advantage of not having a matching parameter Q_0 .

The popularity of the ME+PS method is due to the fact that processes with large jet multiplicity appear often as background of new physics searches. A shower Monte Carlo can simulate the production of events with high jet multiplicity. However, the requirement for jets arising in new physics searches is typically a large transverse momentum and a large separation between jets, as would typically happen in the decay of a very massive object. These kinematical configurations are precisely those where Shower Monte Carlo programs fail to be accurate, since they are designed to represent well only small angle emissions. It is thus mandatory to describe these multi-jet backgrounds using exact tree level matrix element calculations.

The NLO+PS methods extend the accuracy of the generation of the basic process at the Next-to-Leading Order level in QCD. They must thus include the radiation of an extra parton with full tree-level accuracy, since this radiation constitutes a NLO correction to the basic process. They must also include NLO virtual corrections. They can be viewed as an extension of the MEC method with the inclusion of NLO virtual corrections. They are however more general, since they are applicable to processes of arbitrary complexity. Two of these methods are now widely used: the MC@NLO method [75] and the POWHEG method [74, 76].

Several ongoing efforts to extend the accuracy of the ME+PS and NLO+PS approaches can be found in the literature: [77] [78, 79] [22, 80].

NLO+PS generators should be viewed as an improvement upon LO shower generators for a given process. It is thus generally convenient to use NLO+PS generators, when available, with respect to LO ones. They are typically design to improve over available LO generators, so that, besides including NLO QCD corrections, they often have features that the LO generator does not have. They should produce NLO accurate distributions for inclusive quantities, and they generate the hardest jet with tree level accuracy even at large angle. It should be reminded, though, that some shower parameters might have been tuned with leading order generators. Thus, the NLO+PS generator may yield a worse description of the distributions that have been used for tuning. This can typically happen in $2 \rightarrow 1$ process, where GPMCs include MEC, and thus differ from the corresponding NLO+PS approach only by a K factor. In the transverse momentum distribution of the Z boson in Z hadroproduction, for example, the shape of the distribution around the peak depends upon a number of Shower non perturbative parameters, like the shower cut-off, the intrinsic transverse momentum of the incoming parton, and the underlying event model. A GPMC, including MEC, that includes a constant K factor, and that has been tuned to data for this process, may yield a better description of the data than an NLO+PS generator. It may thus be wise to consider tuning also the NLO+PS generators in this region. On the other hand, ME+PS generators should be preferred over NLO+PS ones when one needs an accurate description of hard, large angle emission, beyond the hardest jet. Attempts to merge ME+PS and NLO+PS, in order to get event samples that have the advantage of both approaches have appeared in the MENLOPS approach [81–83].

Several ME+PS implementations use existing matrix element generators, like ALPGEN and MGME, for the calculation of the matrix element, and feed the partonic events through an GPMC like PYTHIA or HERWIG using the Les Houches Interface for User Processes (LHI/LHEF) [60, 84], to complete the genetaration. SHERPA and HERWIG++, also include their own matrix element generator and matching algorithm. NLO+PS implementations either rely upon the MC@NLO program, or upon the new aMC@NLO development [85]. Several POWHEG processes are implemented in the POWHEG BOX framework [86]. These programs provide LHI events to be fed through a GPMC. Again, SHERPA and HERWIG++, also include their own POWHEG implementation for several processes.

1.2 Hadronization Models

In the context of event generators, *hadronization* denotes the process by which a set of partons (*after* showering) is transformed into a set of *primary* hadrons, which may then subsequently decay further. This non-perturbative transition takes place at the *hadronization scale*, Q_{had} , which by construction is identical to the infrared cutoff of the parton shower. In the absence of a first-principles solution to the relevant dynamics, event generators use QCD-inspired phenomenological models to describe this transition.

A main difference with respect to analytical approaches is that the fragmentation functions of MC models are intrinsically defined at the hadronization scale, while the ones used in fixed-order approaches are usually defined at some hard factorization scale, Q_F . Hence the

two kinds of functions will differ at least by the perturbative evolution taking place between Q_F and Q_{had} . Another key difference is that MC models must be fully exclusive (i.e., they must address all particles in the final state explicitly) while analytical models typically sum inclusively over most of the event activity.

Although non-perturbative QCD is not solved, we do have some knowledge of its properties. For instance, Poincaré invariance, unitarity, and causality are all concepts that apply beyond perturbation theory. In addition, lattice QCD (see Sec. XX of this *Review*) provides us a means of making explicit quantitative studies in a genuinely non-perturbative setting, albeit only of certain questions.

An important result in “quenched” lattice QCD² is that the potential of the color dipole field between a charge and an anticharge appears to grow linearly with the separation of the charges, when the separation is greater than about a femtometer. This is known as “linear confinement”, and it forms the starting point for the *string model of hadronization*, discussed below in section 1.2.1.

Insight can also be gained by considering the perturbative evolution equations, in particular their properties at the end of the shower, onto which the hadronization model should match smoothly. Following this line of reasoning, an important observation is that the mass spectrum of separate color-singlet subsystems produced by a QCD shower is independent of the starting scale of that evolution, modulo subleading and momentum conservation effects. This property, labeled “preconfinement” [87], is the starting point for the *cluster model of hadronization*, discussed below in section 1.2.2.

Another important perturbative argument is that the functions on the non-perturbative side must obey evolution equations that compensate that of their perturbative counterparts. However, due to their more complicated and fully exclusive nature, it is generally not possible to enforce such scaling laws automatically in Monte Carlo models of hadronization. One must therefore be aware that the model must be “retuned” by hand if changes are made to the perturbative evolution, in particular if the infrared cutoff is modified. Tuning will be discussed below in section 1.4.

Finally, it should be emphasized that the so-called “parton level” that can be obtained by switching off hadronization in a given event generator, is not a universal concept, since each model defines the hadronization scale differently (e.g., by a cutoff in p_{\perp} , invariant mass, etc., with different tunes using different values for the cutoff). Comparisons to distributions at this level may therefore be used to provide an idea of the overall impact of hadronization corrections within a given model, but should be avoided in the context of physical observables.

1.2.1 The String Model

Starting from early concepts [88], several hadronization models based on strings have been proposed [59]. Of these, the most widely used today is the so-called Lund model [89], implemented in PYTHIA [1, 2]. We shall therefore concentrate on that particular model here, though many of the overall concepts would be shared by any string-inspired method. (A more extended discussion can be found in [89]. Other useful reviews are given in [1, 59, 90, 91].)

Consider two opposite colour charges (e.g., a q and a \bar{q}) moving apart. Linear confinement

²Quenched QCD implies no “dynamical” quarks, i.e., no $g \rightarrow q\bar{q}$ splittings allowed.

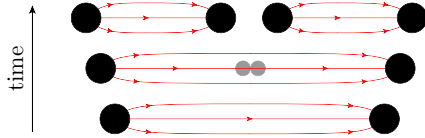


Figure 1.1: Illustration of string breaking by quark pair-creation in the string field.

implies that a potential

$$V(r) = \kappa r \quad (1.7)$$

is reached for large distances, r . (At short distances, there is a Coulomb term $\propto 1/r$ as well, but this is neglected in the Lund model.) This potential describes a string with tension $\kappa \sim 1 \text{ GeV/fm} \sim 0.2 \text{ GeV}^2$. The physical picture is that of a color flux tube being stretched between the q and the \bar{q} .

As the string grows, the non-perturbative creation of quark-antiquark pairs in the string field can break the string, via the process $(q\bar{q}) \rightarrow (q\bar{q}') + (q'\bar{q})$, illustrated in figure 1.1. More complicated multi-parton topologies are treated by representing gluons as transverse “kinks”. Thus soft gluons effectively “build up” a transverse structure in the originally one-dimensional object, with infinitely soft ones smoothly absorbed into the longitudinal string. For strings with finite-energy kinks, the space-time evolution is slightly more involved [89], but the main point is that there are no separate free parameters for gluon jets. Differences with respect to quark fragmentation arise simply because quarks are only connected to a single string piece, while gluons have one on either side, increasing the energy loss (per unit invariant time) from a gluon to the string by a factor of 2 relative to quarks, similar to the ratio of color Casimirs $C_A/C_F = 2.25$.

Since the string breaks are causally disconnected (as can be realized from space-time diagrams [89]), they do not have to be considered in any specific time-ordered sequence. In the Lund model, the string breaks are generated starting with the leading (“outermost”) hadrons, containing the endpoint quarks, and iterating inwards towards the centre of the string, alternating randomly between the left and right sides. One can thereby split off a single on-shell hadron in each step, making it straightforward to ensure that only states consistent with known hadron resonances are produced.

For each breakup vertex, quantum mechanical tunnelling is assumed to control the masses and p_\perp kicks that can be produced, leading to a Gaussian suppression

$$\text{Prob}(m_q^2, p_{\perp q}^2) \propto \exp\left(\frac{-\pi m_q^2}{\kappa}\right) \exp\left(\frac{-\pi p_{\perp q}^2}{\kappa}\right), \quad (1.8)$$

where m_q is the mass of the produced quark flavor and p_\perp is the non-perturbative transverse momentum imparted to it by the breakup process (the antiquark has the same mass and opposite p_\perp), with a universal average value of $\langle p_{\perp q}^2 \rangle = \kappa/\pi \sim (250 \text{ MeV})^2$. The c and b masses are sufficiently heavy that they are not produced at all in the soft fragmentation. The transverse direction is defined with respect to the string axis, so the p_\perp in a frame where the string is moving will be modified by a Lorentz boost factor. Note that the effective amount of “non-perturbative” p_\perp , in a Monte Carlo model with a fixed shower cutoff, may

be larger than the purely non-perturbative κ/π above, to account for effects of additional unresolved soft-gluon radiation below the shower cutoff scale. In principle, the magnitude of this additional component should scale with the cutoff, but in practice it is up to the user to enforce this by retuning this parameter when changing the hadronization scale.

Since quark masses are difficult to define for light quarks, the value of the strangeness suppression is determined from experimental observables, such as the K/π and K^*/ρ ratios. The parton-shower evolution generates a small amount of strangeness as well, through perturbative $g \rightarrow s\bar{s}$ splittings. The optimal value for the non-perturbative $2s/(u+d)$ ratio should therefore exhibit a mild anticorrelation with the amount of quarks produced in the perturbative stage.

Baryon production can also be incorporated, by allowing string breaks to produce pairs of so-called *diquarks*, loosely bound states of two quarks in an overall $\bar{3}$ representation (e.g., $R+B=\bar{G}$). Again, since diquark masses are difficult to define, the relative rate of diquark to quark production is extracted, e.g., from the p/π ratio, and since the perturbative shower splittings do not produce diquarks, the effective value for this parameter is mildly correlated with the amount of $g \rightarrow q\bar{q}$ splittings occurring on the shower side. More advanced scenarios for baryon production have also been proposed, see [89]. Within the PYTHIA framework, a fragmentation model including string junctions [56] is also available and can act to increase baryon number transport from the beam remnant [92].

The next step of the algorithm is assignment of the produced quarks within hadron multiplets. Using a nonrelativistic classification of spin states, the fragmenting q may combine with the \bar{q}' from a newly created breakup to produce a meson — or baryon, if diquarks are involved — of a given valence quark spin S and angular momentum L . The lowest-lying pseudoscalar and vector meson multiplets, and spin-1/2 and -3/2 baryons, are assumed to dominate in a string framework³, but individual rates are not predicted by the model. This is therefore the sector that contains the largest amount of free parameters.

From spin counting, the ratio V/P of vectors to pseudoscalars is expected to be 3, but in practice this is only approximately true for B^*/B . For lighter flavours, the difference in phase space caused by the $V-P$ mass splittings implies a suppression of vector production. When extracting the corresponding parameters from data, it is advisable to begin with the heaviest states, since so-called feed-down from higher-lying hadron states complicates the extraction for lighter particles, see section 1.2.3. For diquarks, separate parameters control the relative rates of spin-1 diquarks vs. spin-0 ones and, likewise, have to be extracted from data.

With p_{\perp}^2 and m^2 now fixed, the final step is to select the fraction, z , of the fragmenting endpoint quark’s longitudinal momentum that is carried by the created hadron, an aspect for which the string model is highly predictive. The requirement that the fragmentation be independent of the sequence in which breakups are considered (causality) imposes a “left-right symmetry” on the possible form of the fragmentation function, $f(z)$, with the solution

³The PYTHIA implementation includes the lightest pseudoscalar and vector mesons, with the four $L=1$ multiplets (scalar, tensor, and 2 pseudovectors) available but disabled by default, largely because several states are poorly known and thus may result in a worse overall description when included. For baryons, the lightest spin-1/2 and -3/2 multiplets are included.

$$f(z) \propto \frac{1}{z}(1-z)^a \exp\left(-\frac{b(m_h^2 + p_{\perp h}^2)}{z}\right), \quad (1.9)$$

which is known as the Lund symmetric fragmentation function (normalized to unit integral). As a by-product, the probability distribution in invariant time τ of $q'\bar{q}$ breakup vertices, or equivalently $\Gamma = (\kappa\tau)^2$, is also obtained, with $dP/d\Gamma \propto \Gamma^a \exp(-b\Gamma)$ implying an area law for the color flux, and the average breakup time lying along a hyperbola of constant invariant time $\tau_0 \sim 10^{-23}\text{s}$ [89]. The a and b parameters are the only free parameters of the fragmentation function, though a may in principle be flavour-dependent. Note that the explicit mass dependence in $f(z)$ implies a harder fragmentation function for heavier hadrons (in the rest frame of the string).

For massive endpoints (e.g., c and b quarks, or hypothetical hadronizing new-physics particles), which do not move along straight lightcone sections, the exponential suppression with string area leads to modifications of the form [93], $f(z) \rightarrow f(z)/z^{bm_Q^2}$, with m_Q the mass of the heavy quark. Strictly speaking, this is the only fragmentation function that is consistent with causality in the string model, though a few alternative forms are typically provided as well.

1.2.2 The Cluster Model

The cluster hadronization model is based on the observation [87, 94] that the color structure of a perturbative QCD shower evolution at any scale Q_0 is such that color singlet subsystems of partons (labeled “clusters”) occur with a universal invariant mass distribution that only depends on Q_0 and on Λ_{QCD} , not on the starting scale Q , for $Q \gg Q_0 \gg \Lambda_{\text{QCD}}$. Further, this mass distribution is power-suppressed at large masses.

Early generator models of hadronization based on this universality include the ones constructed by Field, Fox, and Wolfram [8, 95]. For many years, the cluster model developed by Webber [96] has been a hallmark of the HERWIG and HERWIG++ generators, with an alternative implementation [97] now available in the SHERPA generator. In all cases, the key idea is to enforce “by hand” non-perturbative splitting of all gluons into quark-antiquark pairs at the end of the shower. Compared with the string description, this effectively amounts to viewing the gluons as “seeds” for string breaks, rather than as kinks in a continuous object. After these splittings, a new set of clusters is obtained which contain no perturbative gluons and which have predominantly low invariant masses.

The algorithm starts by assigning flavours and momenta to the quark pairs produced in these forced $g \rightarrow q\bar{q}$ breakups. In the cluster models, constituent quark masses are used, of order $m_{u,d} \sim 300\text{ MeV}$, $m_s \sim 450\text{ MeV}$, with the latter controlling the strangeness suppression in this step. Since these masses are close to the threshold for being pair-produced at all, for a shower cutoff corresponding to a gluon virtuality of $m_g \sim Q_0 \sim 1\text{ GeV}$, the p_{\perp} generated by these splittings is neglected as being much smaller than the overall cluster momenta. The model also allows for (light) diquarks to be produced in these splittings, again with the mass chosen for the diquarks regulating their relative occurrence.

Once these clusters have been formed, the algorithm first decides whether they are sufficiently small to be decayed directly to hadrons, or whether they should first be split into

smaller clusters. For the latter, a sequential binary fission is typically adopted, preserving the orientation along the axis defined by the constituent partons of the original cluster, until the sub-cluster masses fall below some value, typically 3–4 GeV. Due to the preservation of the original axis in these fissions, the initial treatment of high-mass clusters therefore has some resemblance to the string-like picture.

Next, on the low-mass side of the spectrum, some clusters are then allowed to decay directly to a single hadron, with nearby clusters absorbing any excess momentum. This improves the description of the high- z part of the fragmentation spectrum — where the hadron carries almost all the momentum of its parent jet — at the cost of introducing one additional parameter controlling the probability for single-hadron cluster decay.

Having obtained a final distribution of small-mass clusters, now with a strict cutoff at 3–4 GeV and with the component destined to decay to single hadrons already removed, the remaining clusters are interpreted as a smoothed-out spectrum of excited mesons, each of which decays isotropically to two hadrons, with relative probabilities proportional to the available phase space for each possible two-hadron combination that is consistent with the cluster’s internal flavours, including spin degeneracy. It is important that all the light members (containing only uds) of each hadron multiplet be included, as the absence of members can lead to unphysical isospin or SU(3) flavour violation. Typically, the lightest pseudoscalar, vector, scalar, even and odd charge conjugation pseudovector, and tensor multiplets of light mesons are included. In addition, some excited vector multiplets of light mesons may be available. For baryons, usually only the lightest octet, decuplet and singlet baryons are present, although both the HERWIG++ and SHERPA implementations now include some heavier baryon multiplets as well.

Contrary to the case in the string model, the mechanism of phase space suppression employed here leads to a natural enhancement of the lighter pseudoscalars, and no parameters beyond the spectrum of hadron masses need to be introduced at this point. The phase space also limits the transverse momenta of the produced hadrons relative to the jet axis.

Note that, since the masses and decays of excited heavy-flavour hadrons in particular are not well known, there is some freedom in the model to adjust these, which in turn will affect their relative phase-space populations.

1.2.3 Hadron and τ Decays

Of the so-called primary hadrons, originating directly from string breaks and/or cluster decays (see above), many are unstable and so decay further, until a set of particles is arrived at that can be considered stable on time scales relevant to the given measurement⁴. The decay modeling can therefore have a significant impact on final particle yields and spectra, especially for the lowest-lying hadronic states, which receive the largest relative contributions from decays (feed-down). Note that the interplay between primary production and feed-down effectively makes the hadronization tuning (see section 1.4) dependent on the properties of the decay modeling.

Particle summary tables, such as those given elsewhere in this *Review*, represent a con-

⁴E.g., a typical hadron-collider definition of a “stable particle” is $c\tau \geq 10$ mm, which includes the weakly-decaying strange hadrons (K , Λ , Σ^\pm , $\bar{\Sigma}^\pm$, Ξ , Ω).

densed summary of the available experimental measurements and hence may be incomplete and/or exhibit inconsistencies (within the experimental precision). In an MC decay package, on the other hand, all information must be quantified and consistent, with all branching ratios summing to unity. When adapting particle summary information for use in a decay package, a number of choices must therefore be made. The amount of ambiguity increases as more excited meson and baryon multiplets are added to the simulation, about which progressively little is known from experiment. The choices made are generator-specific and are again closely linked to the tuning of hadronization parameters.

A related choice is how to distribute the decay products differentially in phase space, in particular which matrix elements to use. Historically, MC generators contained matrix elements only for selected (generator-specific) classes of hadron and τ decays, coupled with a Breit-Wigner smearing of the masses, truncated at the edges of the physical decay phase space (the treatment of decay thresholds can be important for certain modes [59]). A more sophisticated treatment can then be obtained by reweighting the generated events using the obtained particle four-momenta and/or by using specialized external packages such as EVTGEN [98] for hadron decays and TAUOLA [99] for τ decays.

More recently, HERWIG++ and SHERPA include helicity-dependence in τ decays [100, 101], with a more limited treatment available in PYTHIA 8 [2]. The HERWIG++ and SHERPA generators have also included significantly improved internal simulations of hadronic decays, which include spin correlations between those decays for which matrix elements are used.

HERWIG++ and PYTHIA include the probability for B mesons to oscillate into its antiparticle before it decays. SHERPA and EVTGEN also include CP-violating effects and, for common decay modes of the neutral meson and its antiparticle, the interference between the direct decay and oscillation followed by decay.

Finally, a note of warning on double counting. This may occur if a particle can decay via an intermediate on-shell resonance. An example is $a_1 \rightarrow \pi\pi\pi$ which may proceed via $a_1 \rightarrow \rho\pi$, $\rho \rightarrow \pi\pi$. If these decay channels of the a_1 are both included, each with their full partial width, a double counting of the on-shell $a_1 \rightarrow \rho\pi$ contribution would result. Such cases are normally dealt with consistently in the default MC generator packages, so this warning is mostly intended for users that wish to edit decay tables on their own.

1.3 Models for Soft Hadron-Hadron Physics

1.3.1 Minimum-Bias and Diffraction

The term “minimum bias” originates from the experimental requirement of a minimal number of tracks (or hits) in a given instrumented region. In order to make MC predictions for such observables, all possible contributions to the relevant phase-space region must be accounted for. There are essentially four types of physics processes, which together make up the total hadron-hadron (hh) cross section: 1) elastic scattering (excluding QED⁵): $hh \rightarrow hh$, 2) single diffractive dissociation: $hh \rightarrow h + \text{gap} + X$, with X denoting anything that is not the original beam particle, and “gap” denoting a rapidity region devoid of observed activity; 3) double diffractive dissociation: $hh \rightarrow X + \text{gap} + X$, and 4) inelastic non-diffractive

⁵The QED elastic-scattering cross section diverges and is normally a non-default option in MC models.

scattering: everything else. A fifth class may also be defined, called central diffraction ($hh \rightarrow h + \text{gap} + X + \text{gap} + h$). Some differences exist between theoretical and experimental terminology [102]. In the experimental setting, diffraction is defined by an observable gap, of some minimal size in rapidity. In the MC context, each diffractive physics process typically produces a whole spectrum of gaps, with small ones suppressed but not excluded.

The inelastic non-diffractive part of the cross section is typically modeled either by smoothly regulating and extending the perturbative QCD scattering cross sections all the way to zero p_{\perp} [103] (PYTHIA 6, PYTHIA 8, and SHERPA) or by regulating the QCD cross sections with a sharp cutoff [104] (HERWIG+JIMMY) and adding a separate class of intrinsically soft scatterings below that scale [105] (HERWIG++). In all cases, the three most important ingredients are [106]: 1) the IR regularization of the perturbative scattering cross sections, including their PDF dependence, 2) the assumed transverse mass distribution of the colliding hadrons, possibly including multi-parton correlations [92, 107] and/or x dependence [108], and 3) additional soft-QCD effects such as color reconnections and/or other collective effects. The former two aspects are discussed in section 1.3.2 and the latter in section 1.3.3.

Currently, there are essentially three methods for simulating diffraction in the main MC models: 1) in PYTHIA 6, one picks a diffractive mass according to parametrized cross sections $\propto dM^2/M^2$ [109]. This mass is represented as a string, which is fragmented as described in section 1.2.1, though differences in the effective scale of the hadronization may necessitate a (re)tuning of the fragmentation parameters for diffraction; 2) in PYTHIA 8, the high-mass tail beyond $M \sim 10$ GeV is augmented by a partonic description in terms of pomeron PDFs [110], allowing diffractive jet production including showers and underlying event [111]; 3) the PHOJET program and related models also include central diffraction and rely directly on a formulation in terms of pomerons (color-singlet multi-gluon states) [112–114]. Cut pomerons correspond to exchanges of soft gluons while uncut ones give elastic and diffractive topologies as well as virtual corrections that help preserve unitarity. So-called “hard pomerons” provide a transition to the perturbative regime. Fragmentation is still handled using the Lund string model, so there is some overlap with the above models at the hadronization stage. In addition, an effort is underway to construct an MC implementation of the so-called KMR model [115] within the SHERPA generator. Color reconnections (section 1.3.3) may also play a role in creating rapidity gaps and the underlying event (section 1.3.2) in destroying them.

1.3.2 Underlying Event and Jet Pedestals

In the event-generator context, the term underlying event (UE) denotes any additional activity *beyond* the basic process and its associated ISR and FSR activity. The dominant contribution to this is widely believed to come from additional color exchanges between the remnants, which can be represented either as multiple parton-parton interactions (MPI) or as so-called cut pomerons (section 1.3.1). The experimentally observed fact that the UE is more active than minimum-bias collisions at the same centre-of-mass energy is called the “jet pedestal” effect.

The most easily identifiable consequence of MPI is arguably the possibility of observing several hard parton-parton interactions in one and the same hadron-hadron event. This tends to produce largely uncorrelated back-to-back jet pairs, with each pair having a small value of

$\text{sum}(\vec{p}_\perp)$. For comparison, jets from bremsstrahlung tend to be aligned with the direction of their “parent” partons. The fraction of MPI that give rise to additional reconstructible jets is, however, quite small (how small depends on the exact jet definition used). Additional soft interactions, below the jet cutoff, are much more plentiful, and can give significant corrections to the color flow and total scattered energy of the event. This affects the final-state activity in a more global way, increasing multiplicity and summed E_T distributions, and contributing to the break-up of the beam remnants in the forward direction.

The first detailed Monte Carlo model for perturbative MPI was proposed in [103], and with some variation this still forms the basis for most modern implementations. Some useful additional references can be found in [59]. The first crucial observation is that the t -channel propagators appearing in perturbative QCD $2 \rightarrow 2$ scattering almost go on shell at low p_\perp , causing the differential cross sections to become very large, behaving roughly as:

$$d\hat{\sigma}_{2 \rightarrow 2} \propto \frac{d\hat{t}}{\hat{t}^2} \sim \frac{d\hat{p}_\perp^2}{\hat{p}_\perp^4}, \quad (1.10)$$

This cross section is an inclusive number. Thus, if a single hadron-hadron event contains two parton-parton interactions, it will “count” twice in $\sigma_{2 \rightarrow 2}$ but only once in σ_{tot} , and so on. In the limit that all individual parton-parton interactions are independent and equivalent, one would have

$$\sigma_{2 \rightarrow 2}(p_{\perp \text{min}}) = \langle n \rangle(p_{\perp \text{min}}) \sigma_{\text{tot}}, \quad (1.11)$$

with $\langle n \rangle(p_{\perp \text{min}})$ giving the average of a Poisson distribution in the number of parton-parton interactions above $p_{\perp \text{min}}$ per hadron-hadron collision,

$$\mathcal{P}_n(p_{\perp \text{min}}) = (\langle n \rangle(p_{\perp \text{min}}))^n \frac{\exp(-\langle n \rangle(p_{\perp \text{min}}))}{n!}. \quad (1.12)$$

This simple argument in fact expresses unitarity; instead of the total interaction cross section diverging as $p_{\perp \text{min}} \rightarrow 0$ (which would violate unitarity), we have restated the problem so that it is now the *number of MPI per collision* that diverges, with the total cross section remaining finite. At LHC energies, the $2 \rightarrow 2$ scattering cross sections computed using the full LO QCD cross section folded with modern PDFs becomes larger than the total pp one for p_\perp values of order 4–5 GeV [116]. One therefore expects the average number of perturbative MPI to exceed unity at around that scale.

Two important ingredients remain to fully regulate the remaining divergence. Firstly, the interactions cannot use up more momentum than is available in the parent hadron. This suppresses the large- n tail of the naïve estimate above. In PYTHIA-based models, the multiple interactions are ordered in p_\perp , and the parton distributions for each successive interaction are explicitly constructed so that the sum of x fractions can never be greater than unity. In the HERWIG models, instead the uncorrelated estimate of $\langle n \rangle$ above is used directly as an initial guess, but the actual generation of interactions stop once the energy-momentum conservation limit is exceeded (with the last “offending” interaction also removed from consideration).

The second ingredient suppressing the number of interactions, at low p_\perp and x , is color screening; if the wavelength $\sim 1/p_\perp$ of an exchanged colored parton becomes larger than a typical color-anticolor separation distance, it will only see an *average* color charge that vanishes in the limit $p_\perp \rightarrow 0$, hence leading to suppressed interactions. This screening

effectively provides an infrared cutoff for MPI similar to that provided by the hadronization scale for parton showers. A first estimate of an effective lower cutoff due to color screening would be the proton size

$$p_{\perp\min} \simeq \frac{\hbar}{r_p} \approx \frac{0.2 \text{ GeV} \cdot \text{fm}}{0.7 \text{ fm}} \approx 0.3 \text{ GeV} \simeq \Lambda_{\text{QCD}} , \quad (1.13)$$

but empirically this appears to be far too low. In current models, one replaces the proton radius r_p in the above formula by a “typical color screening distance” d , i.e. an average size of a region within which the net compensation of a given color charge occurs. This number is not known from first principles [115] and is perceived of simply as an effective cutoff parameter. The simplest choice is to introduce a step function $\Theta(p_{\perp} - p_{\perp\min})$. Alternatively, one may note that the jet cross section is divergent like $\alpha_s^2(p_{\perp}^2)/p_{\perp}^4$, cf. eq. (1.10), and that therefore a factor

$$\frac{\alpha_s^2(p_{\perp 0}^2 + p_{\perp}^2)}{\alpha_s^2(p_{\perp}^2)} \frac{p_{\perp 0}^4}{(p_{\perp 0}^2 + p_{\perp}^2)^2} \quad (1.14)$$

would smoothly regulate the divergences, now with $p_{\perp 0}$ as the free parameter. Regardless of whether it is imposed as a smooth (PYTHIA and SHERPA) or steep (HERWIG++) function, this is effectively the main “tuning” parameter in such models.

Note that the numerical value obtained for the cross section depends upon the PDF set used, and therefore the optimal value to use for the cutoff will also depend on this choice. Note also that the cutoff does not have to be energy-independent. Higher energies imply that parton densities can be probed at smaller x values, where the number of partons rapidly increases. Partons then become closer packed and the color screening distance d decreases. The uncertainty on the energy and/or x scaling of the cutoff is a major concern when extrapolating between different collider energies [106].

We now turn to the origin of the observational fact that hard jets appear to sit on top of a higher “pedestal” of underlying activity than events with no hard jets. This is interpreted as a consequence of impact-parameter-dependence: in peripheral collisions, only a small fraction of events contain any high- p_{\perp} activity, whereas central collisions are more likely to contain at least one hard scattering; a high- p_{\perp} triggered sample will therefore be biased towards small impact parameters, b . The ability of a model to describe the shape of the pedestal (e.g., to describe both “minimum-bias” data and UE distributions simultaneously) therefore depends upon its modeling of the b -dependence, and correspondingly the impact-parameter shape constitutes another main tuning parameter.

For each impact parameter, b , the number of interactions \tilde{n} can then still be assumed to be distributed according to eq. (1.12), again modulo momentum conservation, but now with the mean value of the Poisson distribution depending on impact parameter, $\langle \tilde{n}(b) \rangle$.

Finally, there are two perturbative modeling aspects which go beyond the introduction of MPI themselves. In particular, this concerns 1) parton showers off the MPI, and 2) perturbative parton-rescattering effects. Without showers, MPI models would generate very sharp peaks for back-to-back MPI jets, caused by unshowered partons passed directly to the hadronization model. However, with the exception of the oldest PYTHIA 6 model [103], all of the GPMC event-generator models do include such showers [59], and hence should exhibit more realistic (i.e., broader and more decorrelated) MPI jets. On the initial-state side of the

MPI shower issue, the main questions are whether and how correlated multi-parton densities are taken into account and, as discussed previously, how the showers are regulated at low p_{\perp} and/or low x . Although none of the MC models currently impose a rigorous correlated multi-parton evolution, all of them include some elementary aspects. The most significant for parton-level results is arguably momentum conservation, which is enforced explicitly in all the models. The so-called “interleaved” models [92, 117] attempt to go a step further, generating an explicitly correlated multi-parton evolution in which flavour sum rules are imposed to conserve, e.g., the total numbers of valence and sea quarks.

Perturbative rescattering in the final state can occur if partons are allowed to undergo several distinct interactions, with showering activity possibly taking place in-between. This has so far not been studied extensively, but a first exploratory model is available [118]. In the initial state, parton rescattering/recombination effects have so far not been included in any of the GPMC models.

1.3.3 Bose-Einstein and Color-Reconnection Effects

In the context of e^+e^- collisions, Bose-Einstein (BE) correlations have mostly been discussed as a source of uncertainty on high-precision W mass determinations at LEP [119]. In hadron-hadron (and nucleus-nucleus) collisions, however, BE correlations are used extensively to study the space-time structure of hadronizing matter (“femtoscopy”), in particular by the heavy-ion community.

In MC models of hadronization, each string break and/or particle/cluster decay is normally factorized from all other ones. This tremendously reduces the number of variables that must be considered simultaneously, but it also makes the introduction of correlations among particles from different breaks/decays intrinsically difficult to address. Within the string model, a number of semi-classical models [120, 121] are available in PYTHIA 6, one of which (BE₃₂ [121]) is carried over to PYTHIA 8. In these models, the BE effect is mimicked by an attractive interaction between pairs of identical particles in the final state. This “force” acts after the decays of very short-lived particles, like ρ , but before decays of longer-lived ones, like π^0 . The main differences between the variants of this model is the assumed shape of the correlation function and how overall momentum conservation is handled. The limitation to pairwise correlations presumably overestimates higher correlations, while the fact that the decay products of longer-lived particles are not included should act to decrease them.

Alternative models for describing the BE effect, including more physical ones, have also been proposed [122–128], but are so far not available in the standard GPMC generators.

As discussed in section 1.2, leading-color (“planar”) color flows are used to set up the hadronizing systems (clusters or strings) at the hadronization stage. If the systems do not overlap significantly in space and time, subleading-color ambiguities and/or non-perturbative reconnections are expected to be small. However, if the density of displaced color charges is sufficiently high that several systems can overlap significantly in space and time, full-color and/or reconnection effects should become progressively larger.

In the specific context of MPI, a crucial question is how color is neutralized *between* different MPI systems, including the remnants. The large rapidity differences involved imply large invariant masses (though normally low p_{\perp}), and hence large amounts of (soft) particle production. Indeed, in the context of soft-inclusive physics, it is these “inter-system”

strings/clusters which furnish the dominant particle-production mechanism, and hence their modeling is an essential part of the soft-physics description, affecting topics such as minimum-bias/UE multiplicity and p_{\perp} distributions, rapidity gaps, and precision mass measurements. A more comprehensive review of colour-reconnection effects can be found in [59].

1.4 Parameters and Tuning

The main virtue of GPMC event generators is their ability to provide a complete and fully differential picture of collider final states, down to the level of individual particles. This allows them to be used as detailed — albeit approximate — theoretical references for experimental measurements. The achievable accuracy depends both on the inclusiveness of the chosen observable and on the sophistication of the simulation itself. An important driver for the latter is obviously the development of improved theoretical models, discussed in the preceding sections; but it also depends crucially on the available constraints on the remaining free parameters. Using existing data to constrain these is referred to as generator tuning.

Although Monte Carlo models may appear to have a bewildering array of independently adjustable parameters, it is worth noting that most of them only control relatively small (exclusive) details of the event generation. The majority of the (inclusive) physics is determined by only a few, very important ones, such as, e.g., the value of α_s , in the perturbative domain, and the properties of the non-perturbative fragmentation function for massless partons, in the non-perturbative one. One may therefore take a factorized approach, first constraining the perturbative parameters and thereafter the non-perturbative ones, each ordered in a measure of their relative significance to the overall modeling.

Recent years have seen the emergence of automated tools that attempt to reduce the amount of both computer and manpower required for this task [129], for instance by making full generator runs only for a limited set of parameter points, and then interpolating between these to obtain approximations to the generator result for intermediate parameter points. Automating the human expert input is more difficult. In the tools currently on the market, this question is addressed by a combination of input solicited from the generator authors (e.g., which parameters and ranges to consider, which observables constitute a complete set, etc) and the elaborate construction of non-trivial weighting functions that determine how much weight is assigned to each individual bin and to each distribution. The field is still burgeoning, however, and future sophistications are to be expected. Nevertheless, at this point the overall quality of the tunes obtained with automated methods appear to at least be competitive with the manual ones.

A word on sanity. Keep in mind that perturbation theory at LO \times LL is doing well if it gets within 10% of a given IR safe measurement. The advent of NLO Monte Carlos may reduce this number slightly, but only for quantities for which one expects NLO precision. For quantities governed by non-perturbative physics, uncertainties are larger. For some quantities, e.g., ones for which the underlying modeling is known to be poor, an order-of-magnitude agreement or worse may have to be accepted.

We devote the rest of this section to an example of one specific recipe that might be followed in a realistic set-up [130]. For simplicity, we focus only on massless partons and on physics at central rapidities, omitting a few more specialized topics such as quarkonium

production and baryon stopping. This should by no means be considered the only approach to the problem, but should at least help give a clearer idea of the steps involved. Note: steps 5–8 depend explicitly on the PDF set used. Note also: the strong coupling constant and the PDFs need only have leading-order validity. Nevertheless, some improvements aimed at the inclusion of some large next-to-leading effects are sometimes implemented. For instance, with the choice of the QCD Λ parameter $\Lambda_{\text{MC}} = 1.569\Lambda_{\overline{\text{MS}}}$ [131] (for 5 active flavours) the accuracy of angular-ordered shower algorithms for certain observables is improved at the NLL level. The question of LO vs. NLO PDFs is more involved [59, 132, 133].

1. Determine a value for the strong coupling $\alpha_s(M_Z)$ (or, equivalently, Λ_{QCD}), using IR safe observables from $e^+e^- \rightarrow$ hadrons, such as event shapes, in regions in which they are neither dominated by hadronization nor by multiple hard jets. For an LO Monte Carlo, differences with respect to other LO determinations of α_s should be NLO. If different options for the running of α_s are available in the code, these can be explored.

2. Determine values for the IR cutoff for final-state radiation (plus any effective modifications to the shower evolution close to the cutoff) and for the parameters of any massless fragmentation functions that appear in the model. Useful observables include non-perturbatively dominated regions of the observables from step 1 (such as the back-to-back region of event shapes) as well as inclusive particle multiplicities and momentum distributions.

3. Test the scaling of both IR safe and IR sensitive observables from steps 1 and 2 between different e^+e^- centre-of-mass energies.

4. Determine the parameters governing the relative rates of specific particle species in the hadronization and decay model, as a fraction of the total multiplicity. Also consider their individual fragmentation functions, if these are adjustable in the model. Relevant observables include identified-particle fractions and momentum spectra, hadron decay branching ratios, and particle-particle correlations.

5. Determine values for the IR cutoff for initial-state radiation (plus any effective modifications to the shower evolution close to the cutoff) and for “primordial k_T ” from the low- p_\perp peak of the dilepton p_\perp spectrum in Drell-Yan events in hadron-hadron collisions. A compromise on $\alpha_s(M_Z)$ may be required if the value found in step 1 does not succeed in describing the rest of this spectrum.

6. Underlying Event. Determine the IR regularization for MPI, the hadron transverse-mass distribution, and the strength of color reconnections (CR). Observables should be limited to regions “transverse” to hard jets (and/or “underneath” leptons) Salient quantities are the energy sum in such regions, its fluctuations, and distributions of particle multiplicities and average momenta. Note, if the CR strength is significant, this may have to be included also in the e^+e^- tuning, steps 2–4. The tail of semi-hard MPI jets may to some extent also be constrained by measurements of multi-jet pairs, to the extent that MPI-sensitive observables are available for such topologies.

7. If the model contains adjustable parameters for the matching of showers to processes involving initial-final connections, these may be determined, e.g., from comparisons to jet shapes in hadron collisions. Note: step 6 may have to be iterated.

8. If the model includes soft-inclusive QCD, test the parameters determined in step 6 against (diffraction-suppressed) minimum-bias observables, and against the pedestal effect (the rise from minimum-bias to UE, section 1.3.2). If the pedestal shape is badly described, different parameter sets for minimum-bias and UE tunes may have to be accepted.

Bibliography

- [1] T. Sjöstrand, S. Mrenna, and P. Skands, JHEP **05**, 026 (2006), hep-ph/0603175.
- [2] T. Sjöstrand, S. Mrenna, and P. Z. Skands, Comput.Phys.Commun. **178**, 852 (2008), 0710.3820.
- [3] G. Corcella *et al.*, JHEP **0101**, 010 (2001), hep-ph/0011363.
- [4] M. Bahr *et al.*, Eur.Phys.J. **C58**, 639 (2008), 0803.0883.
- [5] T. Gleisberg *et al.*, JHEP **0402**, 056 (2004), hep-ph/0311263.
- [6] T. Kinoshita, J.Math.Phys. **3**, 650 (1962).
- [7] T. Lee and M. Nauenberg, Phys.Rev. **133**, 1549 (1964).
- [8] G. C. Fox and S. Wolfram, Nucl.Phys. **B168**, 285 (1980).
- [9] G. Altarelli and G. Parisi, Nucl.Phys. **B126**, 298 (1977).
- [10] A. Einstein, B. Podolsky, and N. Rosen, Phys.Rev. **47**, 777 (1935).
- [11] B. Webber, Phys.Lett. **B193**, 91 (1987).
- [12] J. C. Collins, Nucl.Phys. **B304**, 794 (1988).
- [13] I. Knowles, Comput.Phys.Commun. **58**, 271 (1990).
- [14] T. Sjöstrand, Phys.Lett. **B157**, 321 (1985).
- [15] A. Bassetto, M. Ciafaloni, and G. Marchesini, Nucl.Phys. **B163**, 477 (1980).
- [16] D. Amati, A. Bassetto, M. Ciafaloni, G. Marchesini, and G. Veneziano, Nucl.Phys. **B173**, 429 (1980).
- [17] A. H. Mueller, Phys.Lett. **B104**, 161 (1981).
- [18] G. Marchesini and B. Webber, Nucl.Phys. **B238**, 1 (1984).
- [19] G. Gustafson, Phys.Lett. **B175**, 453 (1986).
- [20] G. Gustafson and U. Pettersson, Nucl.Phys. **B306**, 746 (1988).

- [21] L. Lonnblad, *Comput.Phys.Commun.* **71**, 15 (1992).
- [22] W. T. Giele, D. A. Kosower, and P. Z. Skands, *Phys.Rev.* **D78**, 014026 (2008), 0707.3652.
- [23] J.-C. Winter and F. Krauss, *JHEP* **0807**, 040 (2008), 0712.3913.
- [24] A. J. Larkoski and M. E. Peskin, *Phys.Rev.* **D81**, 054010 (2010), 0908.2450.
- [25] Z. Nagy and D. E. Soper, *JHEP* **0510**, 024 (2005), hep-ph/0503053.
- [26] Z. Nagy and D. E. Soper, p. 101 (2006), hep-ph/0601021.
- [27] S. Schumann and F. Krauss, *JHEP* **0803**, 038 (2008), 0709.1027.
- [28] E. Norrbin and T. Sjostrand, *Nucl.Phys.* **B603**, 297 (2001), hep-ph/0010012.
- [29] S. Catani, S. Dittmaier, M. H. Seymour, and Z. Trocsanyi, *Nucl.Phys.* **B627**, 189 (2002), hep-ph/0201036.
- [30] L. Lipatov, *Sov.J.Nucl.Phys.* **23**, 338 (1976).
- [31] E. Kuraev, L. Lipatov, and V. S. Fadin, *Sov.Phys.JETP* **45**, 199 (1977).
- [32] I. Balitsky and L. Lipatov, *Sov.J.Nucl.Phys.* **28**, 822 (1978).
- [33] V. S. Fadin and L. Lipatov, *Phys.Lett.* **B429**, 127 (1998), hep-ph/9802290.
- [34] H. Jung and G. P. Salam, *Eur. Phys. J.* **C19**, 351 (2001), hep-ph/0012143.
- [35] H. Jung *et al.*, *Eur.Phys.J.* **C70**, 1237 (2010), 1008.0152.
- [36] M. Ciafaloni, *Nucl.Phys.* **B296**, 49 (1988).
- [37] S. Catani, F. Fiorani, and G. Marchesini, *Phys.Lett.* **B234**, 339 (1990).
- [38] S. Catani, F. Fiorani, and G. Marchesini, *Nucl.Phys.* **B336**, 18 (1990).
- [39] G. Marchesini and B. Webber, *Nucl.Phys.* **B349**, 617 (1991).
- [40] G. Marchesini and B. Webber, *Nucl.Phys.* **B386**, 215 (1992).
- [41] H. Kharraziha and L. Lonnblad, *JHEP* **9803**, 006 (1998), hep-ph/9709424.
- [42] B. Andersson, G. Gustafson, and J. Samuelsson, *Nucl.Phys.* **B467**, 443 (1996), Revised version.
- [43] B. Andersson, G. Gustafson, H. Kharraziha, and J. Samuelsson, *Z.Phys.* **C71**, 613 (1996).
- [44] J. R. Andersen and J. M. Smillie, *JHEP* **1106**, 010 (2011), 1101.5394.
- [45] J. R. Andersen and J. M. Smillie, *Phys.Rev.* **D81**, 114021 (2010), 0910.5113.

- [46] J. R. Andersen and J. M. Smillie, *JHEP* **1001**, 039 (2010), 0908.2786.
- [47] J. R. Andersen, L. Lonnblad, and J. M. Smillie, (2011), 1104.1316.
- [48] C. Flensburg, G. Gustafson, and L. Lonnblad, (2011), 1103.4321, * Temporary entry *.
- [49] A. H. Mueller and B. Patel, *Nucl.Phys.* **B425**, 471 (1994), hep-ph/9403256.
- [50] A. H. Mueller, *Nucl.Phys.* **B415**, 373 (1994).
- [51] A. H. Mueller, *Nucl.Phys.* **B437**, 107 (1995), hep-ph/9408245.
- [52] A. Semenov, *Comput.Phys.Commun.* **180**, 431 (2009), 0805.0555.
- [53] N. D. Christensen and C. Duhr, *Comput.Phys.Commun.* **180**, 1614 (2009), 0806.4194.
- [54] M. Fairbairn *et al.*, *Phys.Rept.* **438**, 1 (2007), hep-ph/0611040.
- [55] H. K. Dreiner, P. Richardson, and M. H. Seymour, *JHEP* **0004**, 008 (2000), hep-ph/9912407.
- [56] T. Sjöstrand and P. Z. Skands, *Nucl.Phys.* **B659**, 243 (2003), hep-ph/0212264.
- [57] P. Richardson and D. Winn, (2011), 1108.6154.
- [58] L. Carloni and T. Sjostrand, *JHEP* **1009**, 105 (2010), 1006.2911.
- [59] A. Buckley *et al.*, *Phys.Rept.* **504**, 145 (2011), 1101.2599.
- [60] J. Alwall *et al.*, *Comput.Phys.Commun.* **176**, 300 (2007), hep-ph/0609017.
- [61] P. Z. Skands *et al.*, *JHEP* **0407**, 036 (2004), hep-ph/0311123.
- [62] J. Alwall *et al.*, (2007), 0712.3311.
- [63] P. Richardson, *JHEP* **0111**, 029 (2001), hep-ph/0110108.
- [64] M. Bengtsson and T. Sjöstrand, *Phys.Lett.* **B185**, 435 (1987).
- [65] M. H. Seymour, *Comput.Phys.Commun.* **90**, 95 (1995), hep-ph/9410414.
- [66] G. Miu and T. Sjostrand, *Phys.Lett.* **B449**, 313 (1999), hep-ph/9812455.
- [67] L. Lonnblad, *Nucl.Phys.* **B458**, 215 (1996), hep-ph/9508261.
- [68] S. Catani, F. Krauss, R. Kuhn, and B. R. Webber, *JHEP* **11**, 063 (2001), hep-ph/0109231.
- [69] F. Krauss, *JHEP* **08**, 015 (2002), hep-ph/0205283.
- [70] L. Lonnblad, *JHEP* **05**, 046 (2002), hep-ph/0112284.

- [71] N. Lavesson and L. Lonnblad, JHEP **04**, 085 (2008), 0712.2966.
- [72] S. Mrenna and P. Richardson, JHEP **05**, 040 (2004), hep-ph/0312274.
- [73] J. Alwall *et al.*, Eur. Phys. J. **C53**, 473 (2008), 0706.2569.
- [74] P. Nason, JHEP **11**, 040 (2004), hep-ph/0409146.
- [75] S. Frixione and B. R. Webber, JHEP **06**, 029 (2002), hep-ph/0204244.
- [76] S. Frixione, P. Nason, and C. Oleari, JHEP **11**, 070 (2007), 0709.2092.
- [77] N. Lavesson and L. Lonnblad, JHEP **12**, 070 (2008), 0811.2912.
- [78] C. W. Bauer, F. J. Tackmann, and J. Thaler, JHEP **12**, 010 (2008), 0801.4026.
- [79] C. W. Bauer, F. J. Tackmann, and J. Thaler, JHEP **12**, 011 (2008), 0801.4028.
- [80] W. T. Giele, D. A. Kosower, and P. Z. Skands, (2011), 1102.2126.
- [81] K. Hamilton and P. Nason, JHEP **1006**, 039 (2010), 1004.1764.
- [82] S. Alioli, K. Hamilton, and E. Re, (2011), 1108.0909, * Temporary entry *.
- [83] F. Siegert, S. Hoche, F. Krauss, and M. Schonherr, PoS **ICHEP2010**, 119 (2010), 1011.6657.
- [84] E. Boos *et al.*, (2001), hep-ph/0109068.
- [85] V. Hirschi *et al.*, JHEP **1105**, 044 (2011), 1103.0621, * Temporary entry *.
- [86] S. Alioli, p. 204 (2010), 1009.2348.
- [87] D. Amati and G. Veneziano, Phys. Lett. **B83**, 87 (1979).
- [88] X. Artru and G. Mennessier, Nucl.Phys. **B70**, 93 (1974).
- [89] B. Andersson *The Lund model* Vol. 7 (Camb. Monogr. Part. Phys. Nucl. Phys. Cosmol., 1997).
- [90] B. Andersson, G. Gustafson, G. Ingelman, and T. Sjöstrand, Phys. Rept. **97**, 31 (1983).
- [91] T. Sjöstrand, (2009), 0911.5286.
- [92] T. Sjöstrand and P. Z. Skands, JHEP **0403**, 053 (2004), hep-ph/0402078.
- [93] M. Bowler, Z.Phys. **C11**, 169 (1981).
- [94] A. Bassetto, M. Ciafaloni, and G. Marchesini, Phys. Lett. **B83**, 207 (1979).
- [95] R. D. Field and S. Wolfram, Nucl.Phys. **B213**, 65 (1983).

- [96] B. Webber, Nucl.Phys. **B238**, 492 (1984).
- [97] J.-C. Winter, F. Krauss, and G. Soff, Eur.Phys.J. **C36**, 381 (2004), hep-ph/0311085.
- [98] D. Lange, Nucl.Instrum.Meth. **A462**, 152 (2001).
- [99] S. Jadach, Z. Was, R. Decker, and J. H. Kuhn, Comput.Phys.Commun. **76**, 361 (1993).
- [100] D. Grellscheid and P. Richardson, (2007), 0710.1951.
- [101] T. Gleisberg *et al.*, JHEP **0902**, 007 (2009), 0811.4622.
- [102] V. Khoze, F. Krauss, A. Martin, M. Ryskin, and K. Zapp, Eur.Phys.J. **C69**, 85 (2010), 1005.4839.
- [103] T. Sjöstrand and M. van Zijl, Phys. Rev. **D36**, 2019 (1987).
- [104] J. M. Butterworth, J. R. Forshaw, and M. H. Seymour, Z. Phys. **C72**, 637 (1996), hep-ph/9601371.
- [105] M. Bähr, J. M. Butterworth, S. Gieseke, and M. H. Seymour, (2009), 0905.4671.
- [106] H. Schulz and P. Skands, Eur.Phys.J. **C71**, 1644 (2011), 1103.3649.
- [107] J. R. Gaunt and W. Stirling, JHEP **1003**, 005 (2010), 0910.4347.
- [108] R. Corke and T. Sjostrand, JHEP **1105**, 009 (2011), 1101.5953, * Temporary entry *.
- [109] G. A. Schuler and T. Sjöstrand, Phys.Rev. **D49**, 2257 (1994).
- [110] G. Ingelman and P. Schlein, Phys.Lett. **B152**, 256 (1985).
- [111] S. Navin, (2010), 1005.3894.
- [112] P. Aurenche *et al.*, Comput.Phys.Commun. **83**, 107 (1994), hep-ph/9402351.
- [113] F. W. Bopp, R. Engel, and J. Ranft, (1998), hep-ph/9803437.
- [114] S. Roesler, R. Engel, and J. Ranft, p. 1033 (2000), hep-ph/0012252.
- [115] M. Ryskin, A. Martin, and V. Khoze, Eur.Phys.J. **C71**, 1617 (2011), 1102.2844, * Temporary entry *.
- [116] M. Bähr, J. M. Butterworth, and M. H. Seymour, JHEP **01**, 065 (2009), 0806.2949.
- [117] T. Sjöstrand and P. Z. Skands, Eur. Phys. J. **C39**, 129 (2005), hep-ph/0408302.
- [118] R. Corke and T. Sjöstrand, JHEP **01**, 035 (2009), 0911.1909.
- [119] LEP Electroweak Working Group, (2005), hep-ex/0511027.
- [120] L. Lönnblad and T. Sjöstrand, Phys.Lett. **B351**, 293 (1995).

- [121] L. Lönnblad and T. Sjöstrand, Eur.Phys.J. **C2**, 165 (1998), hep-ph/9711460.
- [122] M. Biyajima, A. Bartl, T. Mizoguchi, O. Terazawa, and N. Suzuki, Prog.Theor.Phys. **84**, 931 (1990).
- [123] B. Webber, J.Phys.G **G24**, 287 (1998), hep-ph/9708463.
- [124] B. Andersson and M. Ringner, Phys.Lett. **B421**, 283 (1998), hep-ph/9710334.
- [125] S. Jadach and K. Zalewski, Acta Phys.Polon. **B28**, 1363 (1997).
- [126] K. Fialkowski and R. Wit, Acta Phys. Polon. **B28**, 2039 (1997), hep-ph/9709205.
- [127] Q. H. Zhang, U. A. Wiedemann, C. Slotta, and U. W. Heinz, Phys. Lett. **B407**, 33 (1997), nucl-th/9704041.
- [128] S. Mohanty, p. 89 (2002), hep-ph/0211174.
- [129] A. Buckley, H. Hoeth, H. Lacker, H. Schulz, and J. E. von Seggern, Eur.Phys.J. **C65**, 331 (2010), 0907.2973.
- [130] P. Z. Skands, Phys.Rev. **D82**, 074018 (2010), 1005.3457.
- [131] S. Catani, B. Webber, and G. Marchesini, Nucl.Phys. **B349**, 635 (1991).
- [132] A. Sherstnev and R. Thorne, Eur.Phys.J. **C55**, 553 (2008), 0711.2473.
- [133] H.-L. Lai *et al.*, JHEP **1004**, 035 (2010), 0910.4183.